

**SYNTHESIS AND CHARACTERIZATION OF TITANIUM DIOXIDE
NANOTUBES FOR SONOCATALYTIC DEGRADATION OF ORGANIC
DYES IN WASTEWATER**

PANG YEAN LING

UNIVERSITI SAINS MALAYSIA

2013

**SYNTHESIS AND CHARACTERIZATION OF TITANIUM DIOXIDE
NANOTUBES FOR SONOCATALYTIC DEGRADATION OF ORGANIC
DYES IN WASTEWATER**

by

PANG YEAN LING

**Thesis submitted in fulfillment of the
requirements for the degree of
Doctor of Philosophy**

July 2013

ACKNOWLEDGEMENTS

First of all, I would like to express my deepest gratitude to my dedicated supervisor, Associate Professor Dr. Ahmad Zuhairi Abdullah for prestigious guidance, excellent supervision, persistent encouragement, infinite suggestion and invaluable advice rendered throughout this research work. Sincere thanks to him for his patience in reading and correcting the grammatically errors find in my journal paper and thesis even though he is busy with his schedule. I wish to show my sincere thanks to my research co-supervisor, Professor Subhash Bhatia for his capability in shaping up the catalysis research. My accomplishment in this research work is a direct reflection of quality.

I would like to thank all the administrative staffs and laboratories technicians of School of Chemical Engineering for their valuable support, guidance and sincere advices in solving the administrative and technical problems. No doubt, this research work will not to be completed without their helps.

A million thanks goes to my beloved mother and my late father, siblings and soulmate for their infinite support, sincere concern, and endless encouragement and love throughout my research work. Special thanks to all of my beloved friends, colleagues, seniors and juniors for their unselfish help, kindness, motivation and moral support. Thank you all!

Last but not least, the financial support provided by the Research Universiti (RU) Grant, Fellowship Programme and Research Universiti Postgraduate Research

Grant Scheme (USM-RU-PRGS) from Universiti Sains Malaysia are gratefully acknowledged.

Pang Yean Ling

March 2013

TABLE OF CONTENTS

	Page
ACKNOWLEDGEMENTS	ii
TABLE OF CONTENTS	iv
LIST OF TABLES	x
LIST OF FIGURES	xii
LIST OF PLATES	xviii
LIST OF ABBREVIATIONS	xix
LIST OF SYMBOLS	xxii
ABSTRAK	xxvi
ABSTRACT	xxviii
CHAPTER 1 : INTRODUCTION	1
1.1 Water pollution in Malaysia	1
1.2 Dye production, characteristics of textile industry effluent and its environmental impacts	2
1.3 Colour removal techniques	5
1.4 Problem statement	7
1.5 Research objectives	9
1.6 Research scope	10
1.7 Organization of thesis	12
CHAPTER 2 : LITERATURE REVIEW	15
2.1 Fundamentals of ultrasound	15
2.1.1 Sonolytic kinetic mechanism of water molecules	17
2.1.2 Ultrasonic reaction systems	18
2.2 Heterogeneous sonocatalytic degradation using titanium dioxide (TiO ₂)	20
2.3 TiO ₂ nanotubes (NTs) catalyst	23
2.3.1 Formation mechanism of TiO ₂ NTs	27
2.3.2 Post treatment of TiO ₂ NTs	30
2.3.3 Modification of TiO ₂ NTs	33

2.3.4	Characterization of TiO ₂ NTs	39
2.4	Parameter studies	43
2.4.1	Effect of TiO ₂ nanoparticles (NPs) and TiO ₂ NTs	43
2.4.2	Sonocatalytic degradation of various organic dyes	44
2.4.3	Effect of initial concentration of dye	45
2.4.4	Effect of catalyst dosage	46
2.4.5	Effect of solution pH	47
2.4.6	Effect of ultrasonic frequency and ultrasonic power	48
2.4.7	Effect of H ₂ O ₂ dosage	50
2.4.8	Effect of solution temperature	52
2.4.9	Effect of dissolved air	53
2.5	Optimization studies	55
2.5.1	Response surface methodology (RSM)	55
2.5.2	Central composite design (CCD)	55
2.5.3	Model fitting and statistical analysis	56
2.6	Pathways and mechanism for oxidation degradation of Rhodamine B	59
2.7	Catalyst reusability	61
2.8	Reaction kinetic and kinetic model study	62
2.8.1	Model developed by Okitsu's group	63
2.8.2	Model developed by Priya's and Ghows's groups	66
2.9	Concluding remarks	70
CHAPTER 3 : MATERIALS AND METHODOLOGY		71
3.1	Materials and chemicals	71
3.2	Overall experimental flow chart	73
3.3	Experimental setup	75
3.4	Preparation, characterizations and catalytic activities of TiO ₂ catalysts	76
3.4.1	Preparation of catalysts	76
(a)	Preparation of TiO ₂ NPs	76
(b)	Preparation of TiO ₂ NTs	77
(c)	Preparation of C-N codoped TiO ₂ NTs	77
(d)	Preparation of Fe-doped TiO ₂ NTs	78
3.4.2	Characterizations of TiO ₂ catalysts	78

(a)	Scanning electron microscopy (SEM)	78
(b)	Energy dispersive X-ray (EDX)	79
(c)	Transmission electron microscopy (TEM)	79
(d)	X-ray diffraction (XRD)	80
(e)	Raman spectroscopy	81
(f)	Fourier transformed infrared (FT-IR) spectroscopy	81
(g)	Nitrogen adsorption-desorption measurement	82
(h)	UV-vis diffuse reflectance spectroscopy (UV-vis DRS)	83
(i)	Thermal gravimetric analysis-differential thermal analysis (TGA-DTA)	84
(j)	Zeta potential measurement	85
(k)	X-ray photoelectron spectroscopy (XPS)	85
(l)	Elemental analysis (EA)	86
(m)	Atomic absorption flame emission spectroscopy (AAS)	86
3.4.3	Parameter studies in sonocatalytic process	86
(a)	Effect of various TiO ₂ catalysts	87
(b)	Sonocatalytic degradation of various organic dyes	87
(c)	Effect of initial concentration of Rhodamine B	88
(d)	Effect of catalyst dosage	89
(e)	Effect of solution pH	89
(f)	Effect of ultrasonic frequency and ultrasonic power	89
(g)	Effect of H ₂ O ₂ dosage	90
(h)	Effect of solution temperature	91
(i)	Effect of dissolved air	91
3.4.4	Design of experiment (DoE)	91
3.4.5	Sonocatalytic activities of doped TiO₂ NTs	93
(a)	Sonocatalytic activities of C-N codoped TiO ₂ NTs	93
(b)	Sonocatalytic activities of Fe-doped TiO ₂ NTs	94
3.4.6	Identification of intermediate products for sonocatalytic degradation of Rhodamine B	94
(a)	Fourier transformed infrared (FT-IR) spectroscopy	95
(b)	Gas chromatograph coupled with mass spectrometry (GC/MS)	95

3.5	Analysis of liquid samples	96
3.5.1	Measurement of dye concentrations	96
3.5.2	Measurement of chemical oxygen demand (COD)	97
3.6	Catalyst reusability study	97
3.7	Reaction kinetic and kinetic model study	98
3.8	Sonocatalytic degradation of real textile wastewater	100
3.8.1	Adsorption-sonocatalytic degradation of real textile wastewater	100
3.8.2	Analysis of liquid samples	101
CHAPTER 4 : RESULTS AND DISCUSSION		102
4.1	Characterizations and catalytic activities of TiO ₂ NPs and TiO ₂ NTs	102
4.1.1	Characterizations of TiO ₂ NPs and TiO ₂ NTs	102
(a)	Transmission electron microscopy (TEM) and scanning electron microscopy (SEM)	102
(b)	Energy dispersive X-ray (EDX)	107
(c)	X-ray diffraction (XRD)	108
(d)	Raman spectroscopy	111
(e)	Fourier transformed infrared (FT-IR) spectroscopy	113
(f)	Nitrogen adsorption-desorption measurement	115
(g)	UV-vis diffuse reflectance spectroscopy (UV-vis DRS)	119
(h)	Thermal gravimetric analysis-differential thermal analysis (TGA-DTA)	121
(i)	Zeta potential measurement	124
4.1.2	Parameter studies in sonocatalytic process	125
(a)	Effect of various TiO ₂ catalysts	125
(b)	Sonocatalytic degradation of various organic dyes	129
(c)	Effect of initial concentration of Rhodamine B	133
(d)	Effect of catalyst dosage	135
(e)	Effect of solution pH	137
(f)	Effect of ultrasonic frequency and ultrasonic power	139
(g)	Effect of H ₂ O ₂ dosage	142
(h)	Effect of solution temperature	143

(i)	Effect of dissolved air	145
4.1.3	Design of experiment (DoE)	148
(a)	Model fitting and statistical analysis	148
(b)	Influence of individual effect	152
(c)	Analysis of response surfaces on factor interactions	153
(d)	Process optimization of the sonocatalytic degradation of Rhodamine B	157
4.2	Characterizations and catalytic activities of C-N codoped TiO ₂ NTs	158
4.2.1	Characterizations of C-N codoped TiO ₂ NTs	158
(a)	Scanning electron microscopy (SEM) and transmission electron microscopy (TEM)	159
(b)	Energy dispersive X-ray (EDX)	161
(c)	Elemental analysis (EA)	162
(d)	X-ray diffraction (XRD)	163
(e)	Fourier transformed infrared (FT-IR) spectroscopy	164
(f)	Nitrogen adsorption-desorption measurement	166
(g)	UV-vis diffuse reflectance spectroscopy (UV-vis DRS)	168
(h)	Thermal gravimetric analysis-differential thermal analysis (TGA-DTA)	171
(i)	X-ray photoelectron spectroscopy (XPS)	173
4.2.2	Sonocatalytic activities of C-N codoped TiO ₂ NTs	177
4.3	Characterizations and catalytic activities of Fe-doped TiO ₂ NTs	179
4.3.1	Characterization of Fe-doped TiO ₂ NTs	179
(a)	Scanning electron microscopy (SEM) and transmission electron microscopy (TEM)	179
(b)	Energy dispersive X-ray (EDX)	182
(c)	Atomic absorption flame emission spectroscopy (AAS)	183
(d)	X-ray diffraction (XRD)	183
(e)	Fourier transformed infrared (FT-IR) spectroscopy	185
(f)	Nitrogen adsorption-desorption measurement	186
(g)	UV-vis diffuse reflectance spectroscopy (UV-vis DRS)	188
(h)	Thermal gravimetric analysis-differential thermal analysis (TGA-DTA)	190

(i) X-ray photoelectron spectroscopy (XPS)	192
4.3.2 Sonocatalytic activities of Fe-doped TiO ₂ NTs	195
4.3.3 Possible mechanism for sonocatalytic activation of Fe-doped TiO ₂ NTs	197
4.3.4 Identification of intermediate products for sonocatalytic degradation of Rhodamine B	200
4.4 Catalyst reusability study	204
4.4.1 Characterizations and sonocatalytic activities of the used TiO ₂ NTs	204
4.4.2 Characterizations and sonocatalytic activities of the used Fe-doped TiO ₂ NTs	211
4.5 Reaction kinetic and kinetic model study	217
4.6 Sonocatalytic degradation of real textile wastewater	225
4.6.1 Effect of simultaneous and consecutive adsorption and sonocatalytic systems	225
4.6.2 Effect of reaction conditions on the sonocatalytic degradation process	227
(a) Effect of solution pH	227
(b) Effect of catalyst dosage	229
(c) Effect of H ₂ O ₂ dosage	231
(d) Effect of adsorption and ultrasonic irradiation time	233
CHAPTER 5 : CONCLUSIONS AND RECOMMENDATIONS	238
5.1 Conclusions	238
5.2 Recommendations	240
REFERENCES	242
APPENDICES	
LIST OF PUBLICATIONS	

LIST OF TABLES

	Page
Table 1.1 Typical characteristics of wastewater from a textile dyeing process and maximum effluent parameter limits for Standards A and B.	3
Table 1.2 Chemical structures and classifications of organic dyes used in this study (Tangestaninejad <i>et al.</i> , 2008; Jamalluddin and Abdullah, 2011).	4
Table 2.1 Sonocatalytic degradation of recalcitrant organic compounds by TiO ₂ -based catalysts.	21–22
Table 2.2 Comparison of available methods for TiO ₂ NTs preparation (Ou and Lo, 2007).	25
Table 2.3 TiO ₂ NTs modified with non-metal ions.	34
Table 2.4 TiO ₂ NTs modified with metal ions.	35
Table 3.1 List of chemicals and reagents used in this research work.	72
Table 3.2 Characteristics of textile wastewater.	73
Table 3.3 Actual values of the variables for their coded levels used in CCD.	90
Table 3.4 Experimental matrix of CCD.	91
Table 3.5 Summary of rate law and rate equations for zero, first and second order reactions (Hung <i>et al.</i> , 2008a).	99
Table 4.1 XRD results of the annealed TiO ₂ NTs.	108
Table 4.2 BET surface area, pore size and pore volume of the annealed TiO ₂ NTs.	115
Table 4.3 Weight losses (%) of TiO ₂ NPs and TiO ₂ NTs at different temperature ranges as determined using TGA.	123
Table 4.4 Rate coefficients for the sonocatalytic degradation of Rhodamine B under various conditions.	128
Table 4.5 Experimental matrix of CCD and experimental results	149
Table 4.6 Results of ANOVA for sonocatalytic degradation efficiency of Rhodamine B.	150

Table 4.7	Optimization criteria at desired goal for sonocatalytic degradation of Rhodamine B.	157
Table 4.8	Results of the experiments after 3 h for model validation conducted at the optimum conditions as obtained from RSM.	157
Table 4.9	Elemental analysis of C-N codoped TiO ₂ NTs with different dopant concentrations.	162
Table 4.10	BET surface area, pore size and pore volume of the C-N codoped-TiO ₂ NTs with different dopant concentrations.	168
Table 4.11	Weight losses (%) of C-N codoped TiO ₂ NTs with different dopant concentrations as determined using TGA.	172
Table 4.12	Iron content in Fe-doped TiO ₂ NTs with different dopant concentrations.	183
Table 4.13	BET surface area, pore size and pore volume of the Fe doped-TiO ₂ NTs with different dopant concentrations.	188
Table 4.14	Weight losses (%) of Fe-doped TiO ₂ NTs with different dopant concentrations as determined using TGA.	192
Table 4.15	Intermediate products of the sonocatalytic degradation of Rhodamine B as detected by GC/MS (Initial dye concentration of 50 mg/L; Fe-doped TiO ₂ NTs catalyst dosage of 2 g/L; solution pH 7; ultrasonic power of 50 W; ultrasonic frequency of 35 kHz; solution temperature of 45 ± 2 °C; H ₂ O ₂ dosage of 8 mM; air flow of 1 L/min; irradiation time of 2 h).	203–204
Table 4.16	BET surface area, pore size and pore volume of the reused TiO ₂ NTs-300.	209
Table 4.17	Iron content in the reused Fe-doped TiO ₂ NTs samples.	214
Table 4.18	Rate coefficients for the sonocatalytic degradation of Rhodamine B with various TiO ₂ catalysts.	218
Table 4.19	Langmuir-Hinshelwood parameters of the ultrasonic degradation of Rhodamine B.	224
Table 4.20	Comparative survey of the sonocatalytic degradation of Rhodamine B in aqueous solution.	237

LIST OF FIGURES

	Page
Figure 1.1 River water quality trend in Malaysia between 2007–2011 (Department of Environment, 2011).	1
Figure 2.1 Graphical summary of the event of bubble formation, bubble growth and subsequent collapse over several acoustic cycles (Leong <i>et al.</i> , 2011).	15
Figure 2.2 Formation, growth and implosion of cavitation bubble in aqueous solution with ultrasonic irradiation bubbles (Suslick, 1989).	16
Figure 2.3 Schematic representations of effective reaction zone in cavitation bubbles (Morel <i>et al.</i> , 2008).	20
Figure 2.4 The structure models of anatase TiO_2 (Nian and Teng, 2006), $\text{H}_2\text{Ti}_3\text{O}_7$ (Chen <i>et al.</i> , 200a), $\text{H}_2\text{Ti}_2\text{O}_5\text{H}_2\text{O}$ (Nian and Teng, 2006) and lepidocrocite-type titanate $\text{H}_x\text{Ti}_{2-x/4}\text{V}_{x/4}\text{O}_4$ ($x \sim 0.7$, V represents vacancy) (Ma <i>et al.</i> , 2003).	26
Figure 2.5 Schemes of three possible mechanisms for multi-walled TiO_2 NTs formation (Bavykin <i>et al.</i> , 2004).	27
Figure 2.6 Schematic diagrams of (a) formation process of nanotube $\text{Na}_2\text{Ti}_2\text{O}_4(\text{OH})_2$ and (b) mechanism for breaking of $\text{H}_2\text{Ti}_2\text{O}_4(\text{OH})_2$ nanotube (Zhang <i>et al.</i> , 2004b).	30
Figure 2.7 Schematic representation of the thermal transformations pathways as a function of sodium content in TiO_2 NTs (Morgado Jr <i>et al.</i> , 2006).	32
Figure 2.8 Model structures for substitutional and interstitial N-dopants in anatase TiO_2 phase (Di Valentin <i>et al.</i> , 2005).	38
Figure 2.9 Electronic band structures for substitutional and interstitial N-dopants in anatase TiO_2 phase computed by Perdew-Burke-Ernzerhof calculations (Di Valentin <i>et al.</i> , 2005).	39
Figure 2.10 CCD for the optimization of (a) two variables (α is 1.41) and (b) three variables (α is 1.68). (Filled, open circle and open square symbols indicated points of factorial design, axial points and center point, respectively) (Aslan, 2008).	56
Figure 2.11 Proposed photocatalytic degradation pathway of Rhodamine B (Yu <i>et al.</i> 2009b).	60

Figure 2.12	(a) Equilibrium of organic pollutant/substrate toward gas/liquid interface before the collapse of the bubble and (b) sonolytic degradation of organic pollutant/substrate in an effective reaction zone after the collapse of the bubble (Okitsu <i>et al.</i> , 2009).	64
Figure 3.1	Flow chart of the overall research activities involved in this study.	74
Figure 3.2	Schematic diagram of the sonocatalytic experimental setup.	76
Figure 4.1	EDX spectrum of (a) TiO ₂ NTs-0 and (b) TiO ₂ NTs-300.	107
Figure 4.2	XRD pattern of (a) TiO ₂ NPs (b) TiO ₂ NTs-0, (c) TiO ₂ NTs-300, (d) TiO ₂ NTs-500, (e) TiO ₂ NTs-700 and (f) TiO ₂ NTs-900.	109
Figure 4.3	Raman spectra of (a) TiO ₂ NPs (b) TiO ₂ NTs-0, (c) TiO ₂ NTs-300, (d) TiO ₂ NTs-500, (e) TiO ₂ NTs-700 and (f) TiO ₂ NTs-900.	112
Figure 4.4	FT-IR spectra of (a) TiO ₂ NPs (b) TiO ₂ NTs-0, (c) TiO ₂ NTs-300, (d) TiO ₂ NTs-500, (e) TiO ₂ NTs-700 and (f) TiO ₂ NTs-900.	114
Figure 4.5	Pore size distribution of various annealed TiO ₂ catalysts.	117
Figure 4.6	Nitrogen adsorption-desorption isotherm on the surface of (a) TiO ₂ NPs (b) TiO ₂ NTs-0, (c) TiO ₂ NTs-300, (d) TiO ₂ NTs-500, (e) TiO ₂ NTs-700 and (f) TiO ₂ NTs-900.	118
Figure 4.7	(a) UV-vis diffuse reflectance spectra and (b) band gap energy of various annealed TiO ₂ catalysts.	120
Figure 4.8	TGA-DTA curves of the (a) TiO ₂ NPs, (b) TiO ₂ NTs-0 and (c) TiO ₂ NTs-300.	122
Figure 4.9	Zeta potential for TiO ₂ NPs and TiO ₂ NTs-300 at different pH values.	124
Figure 4.10	(a) Degradation efficiency of Rhodamine B versus irradiation times for TiO ₂ NPs and various annealed TiO ₂ NTs and (b) Apparent first-order kinetic plots for sonocatalytic degradation of Rhodamine B (Initial dye concentration of 50 mg/L; TiO ₂ catalyst dosage of 2 g/L; solution pH 7; ultrasonic power of 50 W; ultrasonic frequency of 35 kHz; solution temperature of 30 ± 2 °C).	127

Figure 4.11	Degradation efficiency of various organic dyes (a) without catalyst and (b) with TiO ₂ NTs-300. (Initial dye concentration of 50 mg/L; TiO ₂ NTs-300 catalyst dosage of 2 g/L; solution pH 7; ultrasonic power of 50 W; ultrasonic frequency of 35 kHz; solution temperature of 30 ± 2 °C).	130
Figure 4.12	Effect of initial dye concentration on sonocatalytic degradation of Rhodamine B (TiO ₂ NTs-300 catalyst dosage of 2 g/L; solution pH 7; ultrasonic power of 50 W; ultrasonic frequency of 35 kHz; solution temperature of 30 ± 2 °C).	134
Figure 4.13	Effect of TiO ₂ NTs-300 dosage on sonocatalytic degradation of Rhodamine B (Initial dye concentration of 50 mg/L; solution pH 7; ultrasonic power of 50 W; ultrasonic frequency of 35 kHz; solution temperature of 30 ± 2 °C).	136
Figure 4.14	Effect of solution pH on sonocatalytic degradation of Rhodamine B (Initial dye concentration of 50 mg/L; TiO ₂ NTs-300 catalyst dosage of 2 g/L; ultrasonic power of 50 W; ultrasonic frequency of 35 kHz; solution temperature of 30 ± 2 °C).	138
Figure 4.15	Effect of ultrasonic power and ultrasonic frequency on sonocatalytic degradation of Rhodamine B (Initial dye concentration of 50 mg/L; TiO ₂ NTs-300 catalyst dosage of 2 g/L; solution pH 7; solution temperature of 30 ± 2 °C).	140
Figure 4.16	Effect of addition amount of H ₂ O ₂ on sonocatalytic degradation of Rhodamine B (Initial dye concentration of 50 mg/L; TiO ₂ NTs-300 catalyst dosage of 2 g/L; solution pH 7; ultrasonic power of 50 W; ultrasonic frequency of 35 kHz; solution temperature of 30 ± 2 °C).	142
Figure 4.17	Effect of solution temperature on sonocatalytic degradation of Rhodamine B (Initial dye concentration of 50 mg/L; TiO ₂ NTs-300 catalyst dosage of 2 g/L; solution pH 7; ultrasonic power of 50 W; ultrasonic frequency of 35 kHz; H ₂ O ₂ dosage of 8 mM).	144
Figure 4.18	Effect of the presence of dissolved air on the sonolysis and sonocatalytic degradation of Rhodamine B (Initial dye concentration of 50 mg/L; TiO ₂ NTs-300 catalyst dosage of 2 g/L; solution pH 7; ultrasonic power of 50 W; ultrasonic frequency of 35 kHz; solution temperature of 45 ± 2 °C; H ₂ O ₂ dosage of 8 mM; air flow of 1 L/min)	146
Figure 4.19	Actual and predicted values of sonocatalytic degradation of Rhodamine B.	151

Figure 4.20	The individual effect of (a) initial concentration of Rhodamine B (b) catalyst dosage and (c) power of ultrasonic irradiation on the degradation of Rhodamine B.	153
Figure 4.21	The three-dimensional plots for the degradation efficiency (%) of Rhodamine B to analyze the interactions between (a) initial dye concentration and catalyst loading at ultrasonic power of 60 W (b) initial dye concentration and ultrasonic power at catalyst loading of 2 g/L and (c) catalyst loading and ultrasonic power on initial dye concentration of 50 mg/L.	154
Figure 4.22	EDX spectrum of C-N0.3 codoped TiO ₂ NTs.	162
Figure 4.23	XRD patterns of C-N codoped TiO ₂ NTs prepared with different dopant concentrations.	164
Figure 4.24	FT-IR spectra of C-N codoped TiO ₂ NTs prepared with different dopant concentrations.	165
Figure 4.25	Nitrogen adsorption-desorption isotherm and (b) pore size distribution of C-N codoped TiO ₂ NTs prepared with different dopant concentrations.	167
Figure 4.26	(a) UV-vis diffuse reflectance spectra and (b) band gap energy of C-N codoped TiO ₂ NTs prepared with different dopant concentrations.	170
Figure 4.27	(a) TGA (b) DTA curves of C-N codoped TiO ₂ NTs with different dopant concentrations.	172
Figure 4.28	XPS spectra of C-N0.3 codoped TiO ₂ NTs (a) survey, (b) C 1s peaks, (c) N 1s peaks, (d) Ti 2p peaks, (e) O 1s peaks and (f) Na 1s peaks.	174
Figure 4.29	Degradation of Rhodamine B versus irradiation time for C-N codoped TiO ₂ NTs with different dopant concentrations (Initial dye concentration of 50 mg/L; C-N codoped TiO ₂ NTs catalyst dosage of 2 g/L; solution pH 7; ultrasonic power of 50 W; ultrasonic frequency of 35 kHz; solution temperature of 45 ± 2 °C; H ₂ O ₂ dosage of 8 mM; air flow of 1 L/min).	178
Figure 4.30	EDX spectrum of Fe0.005-doped TiO ₂ NTs.	182
Figure 4.31	XRD patterns of (a) Fe0.001 (b) Fe0.005, (c) Fe0.01 and Fe0.02-doped TiO ₂ NTs.	184
Figure 4.32	FT-IR spectra of Fe-doped TiO ₂ NTs with different dopant concentrations.	185

Figure 4.33	Nitrogen adsorption-desorption isotherm and (b) pore size distribution of Fe-doped TiO ₂ NTs with different dopant concentrations.	187
Figure 4.34	(a) UV-vis diffuse reflectance spectra and (b) band gap energy of Fe-doped TiO ₂ NTs with different dopant concentrations.	189
Figure 4.35	(a) TGA (b) DTA curves of Fe-doped TiO ₂ NTs with different dopant concentrations.	191
Figure 4.36	XPS spectra of Fe0.005-doped TiO ₂ NTs (a) survey (b) Ti 2p peaks (c) O 1s peaks (d) Fe 2p peaks and (e) Na 1s peaks.	193
Figure 4.37	Degradation of Rhodamine B versus irradiation time for Fe-doped TiO ₂ NTs with different dopant concentrations (Initial dye concentration of 50 mg/L; Fe-doped TiO ₂ NTs catalyst dosage of 2 g/L; solution pH 7; ultrasonic power of 50 W; ultrasonic frequency of 35 kHz; solution temperature of 45 ± 2 °C; H ₂ O ₂ dosage of 8 mM; air flow of 1 L/min).	196
Figure 4.38	Mechanism for the synergistic effect of Fe-doped TiO ₂ NTs in the sonocatalytic degradation process.	198
Figure 4.39	The FT-IR spectra of (a) Rhodamine B and (b) degraded dye after 2 h of ultrasonic irradiation (Initial dye concentration of 50 mg/L; Fe-doped TiO ₂ NTs catalyst dosage of 2 g/L; solution pH 7; ultrasonic power of 50 W; ultrasonic frequency of 35 kHz; solution temperature of 45 ± 2 °C; H ₂ O ₂ dosage of 8 mM; air flow of 1 L/min).	201
Figure 4.40	EDX spectrum of reused TiO ₂ NTs-300-4.	207
Figure 4.41	XRD pattern of TiO ₂ NTs-300 after ultrasonic irradiation for (a) 3h, (b) 6 h, (c) 9 h and (d) 12 h.	208
Figure 4.42	Pore size distribution for the reused TiO ₂ NTs-300.	209
Figure 4.43	Degradation efficiency of Rhodamine B versus irradiation times for the reused TiO ₂ NTs-300 for 3 h.	210
Figure 4.44	EDX spectrum of reused Fe0.005-doped TiO ₂ NTs-4.	214
Figure 4.45	TGA curves for the reused Fe0.005-doped TiO ₂ NTs.	215
Figure 4.46	Degradation efficiency of Rhodamine B versus irradiation times for the reused Fe0.005-doped TiO ₂ NTs.	216

Figure 4.47	Apparent first-order kinetic plots for sonocatalytic degradation of Rhodamine B using various TiO_2 catalysts (Initial dye concentration of 50 mg/L; TiO_2 catalyst dosage of 2 g/L; solution pH 7; ultrasonic power of 50 W; ultrasonic frequency of 35 kHz; solution temperature of $45 \pm 2^\circ\text{C}$; H_2O_2 dosage of 8 mM; air flow of 1 L/min).	218
Figure 4.48	Kinetic of sonocatalytic degradation efficiency of Rhodamine B (a) without catalyst, (b) with TiO_2 NPs, (c) with TiO_2 NTs-300 (d) with C-N0.3 TiO_2 NTs and (e) with Fe0.005 TiO_2 NTs (Initial dye concentration of 50 mg/L; TiO_2 catalyst dosage of 2 g/L; solution pH 7; ultrasonic power of 50 W; ultrasonic frequency of 35 kHz).	219
Figure 4.49	Arrhenius plot of rate constant versus reciprocal of reaction temperature for ultrasonic degradation of Rhodamine B without and with various catalysts.	221
Figure 4.50	Sonocatalytic degradation efficiency of Rhodamine B (a) without catalyst, (b) with TiO_2 NPs, (c) with TiO_2 NTs-300, (d) C-N0.3 codoped TiO_2 NTs and (e) Fe0.005-doped TiO_2 NTs after 30 min of adsorption (TiO_2 catalyst dosage of 2 g/L; solution pH 7; ultrasonic power of 50 W; ultrasonic frequency of 35 kHz; solution temperature of $30 \pm 2^\circ\text{C}$).	223
Figure 4.51	Reciprocal plot of initial rate of ultrasonic degradation versus initial dye concentration of Rhodamine B.	224
Figure 4.52	Degradation efficiency of (a) COD and (b) colour without and with different catalysts under ultrasonic irradiation (Solution pH 3, catalyst dosage of 6 g/L, temperature of $30 \pm 2^\circ\text{C}$, reaction time of 3 h).	226
Figure 4.53	Effect of solution pH on (a) COD and (b) colour degradation efficiencies (Catalyst dosage of 6 g/L, temperature of $30 \pm 2^\circ\text{C}$, reaction time of 3 h).	228
Figure 4.54	Effect of catalyst dosage on (a) COD and (b) colour degradation efficiencies (Solution pH 3, temperature of $30 \pm 2^\circ\text{C}$, reaction time of 3 h).	230
Figure 4.55	Effect of H_2O_2 dosage on (a) COD and (b) colour degradation efficiencies (Solution pH 3, catalyst dosage of 6 g/L, temperature of $30 \pm 2^\circ\text{C}$, reaction time of 3 h).	232
Figure 4.56	(a) Effect of adsorption and ultrasonic irradiation on the degradation efficiencies of COD, colour and TOC and, (b) kinetic plots for degradation efficiencies of COD, colour and TOC (Solution pH 3, catalyst dosage of 6 g/L, temperature of $30 \pm 2^\circ\text{C}$, H_2O_2 dosage of 40 mM, aeration).	234

LIST OF PLATES

	Page	
Plate 4.1	TEM images of (a) TiO ₂ NPs (b) TiO ₂ NTs-0, (c) TiO ₂ NTs-300, (d) TiO ₂ NTs-500, (e) TiO ₂ NPs-700 and (f) TiO ₂ NPs-900.	104
Plate 4.2	SEM images of (a) TiO ₂ NPs (b) TiO ₂ NTs-0, (c) TiO ₂ NTs-300, (d) TiO ₂ NTs-500, (e) TiO ₂ NPs-700 and (f) TiO ₂ NPs-900 (magnification: 30,000 x).	105
Plate 4.3	SEM images of (a) C-N0.1, (b) C-N0.3, (c) C-N0.5, (d) C-N1.0 codoped TiO ₂ NTs (magnification: 50,000 x).	160
Plate 4.4	TEM images of (a) TiO ₂ NTs-300 (high-magnification), (b) C-N0.3 codoped TiO ₂ NTs (low-magnification) and (c) C-N0.3 codoped TiO ₂ NTs (high-magnification).	161
Plate 4.5	SEM images of (a) Fe0.001, (b) Fe0.005, (c) Fe0.01 and (d) Fe0.02-doped TiO ₂ NTs (magnification: 50,000 x).	181
Plate 4.6	TEM images of Fe0.005-doped TiO ₂ NTs at (a) low- and (b) high- magnifications.	182
Plate 4.7	SEM images of TiO ₂ NTs-300 after ultrasonic irradiation for (a) 3 h, (b) 6 h, (c) 9 h and (d) 12 h (magnification: 30,000 x).	207
Plate 4.8	TEM images of TiO ₂ NTs-300 after ultrasonic irradiation for (a) 3 h, (b) 6 h, (c) 9 h and (d) 12 h.	208
Plate 4.9	SEM images of Fe0.005-doped TiO ₂ NTs after ultrasonic irradiation for (a) 3 h, (b) 6 h, (c) 9 h and (d) 12 h (magnification: 50,000 x).	214
Plate 4.10	TEM images of Fe0.005-doped TiO ₂ NTs after ultrasonic irradiation for (a) 3 h, (b) 6 h, (c) 9 h and (d) 12 h.	215

LIST OF ABBREVIATIONS

Symbol	Description
a. u.	Arbitrary unit
AAS	Atomic absorption flame emission spectroscopy
AF	Azo fuchsine
ANOVA	Analysis of variance
AOPs	Advanced oxidation processes
ARB	Acid Red B
at.	Atomic percentage
BB 41	Basic Blue 41
BET	Brunauer-Emmett-Teller
BJH	Barrett-Joyner-Halenda
BOD	Biochemical oxygen demand
CCD	Central composite design
CMP	2-chloro-5-methyl phenol
COD	Chemical oxygen demand
DoE	Design of experiment
EA	Elemental analysis
EDX	Energy dispersive X-ray
e.g.	For example
1D	One-dimensional
2D	Two-dimensional
3D	Three-dimensional
FT-IR	Fourier transformed infrared spectroscopy

GC/MS	Gas chromatograph coupled with mass spectrometry
HPLC	High performance liquid chromatography
i.e.	That is
IUPAC	International Union of Pure and Applied Chemistry
LC/MS	Liquid chromatograph method coupled with mass spectroscope
MB	Methylene Blue
MO	Methyl Orange
MP	Methyl parathion
n.d.	No data
NPs	Nanoparticles
NTs	Nanotubes
P	Product/ intermediate product
Prob > <i>F</i>	Probability of seeing the observed <i>F</i> value if the null hypothesis is true
pzc	Point of zero charge
RB5	Reactive Black 5
RSM	Response surface methodology
S	Substrate
SEM	Scanning electron microscopy
TEM	Transmission electron microscopy
TGA-DTA	Thermal gravimetric analysis-differential thermal analysis
TOC	Total organic carbon
UV	Ultraviolet
UV-vis DRS	UV-vis diffuse reflectance spectroscopy
wt.	Weight percentage

XRD	X-ray diffraction
XPS	X-ray photoelectron spectroscopy

LIST OF SYMBOLS

Symbols	Descriptions	Unit
α	The distance of the axial point from center point in CCD	Dimensionless
α_a	Absorption coefficient of the semiconductor material	(m ⁻¹)
A	Arrhenius factor (pre-exponential factor)	Dimensionless
A_a	Absorption constant of the semiconductor material	(m ⁻¹)
β	Full width at half maximum of selected peak	Radians
$\beta_o, \beta_i, \beta_{ii}$ and β_{ij}	Constant, linear, quadratic and interaction coefficients	Dimensionless
c	Velocity of light	(m/s)
C_0	Initial concentration of organic pollutant	(mg/L)
C_t	Concentration of dye at time, t	(mg/L)
$-\frac{dC}{dt}$	Differential of concentration of organic pollutant with respect to time (t)	(mg/L.min)
D	Dye molecule	Dimensionless
D_c	Average size of crystallite	(m)
e^-	Electron	Dimensionless
E_a	Activation energy	(kJ/mol)
E_g	Band gap energy	(eV)
ε	Standard error	Dimensionless
$F\text{-value}$	Ratio of model mean square to residuals mean square	Dimensionless
γ	Specific heat ratio of the gas/vapor mixture	Dimensionless
h	Planck constant	eVs

h^+	Hole	Dimensionless
hv	Photon energy	(eV)
I_A	Intensity of anatase reflection	(Counts/s)
I_R	Intensity of rutile reflection	(Counts/s)
k	Apparent reaction rate constant used in the Langmuir-Hinshelwood model	(mg/L.min)
k'	Rate constant for oxidation Rhodamine B by $\bullet\text{OH}$	(min ⁻¹)
K	Equilibrium constant	(L/mg)
k_1	Rate constant of adsorption of organic pollutant from the bulk solution to the interfacial region of cavitation bubbles	(min ⁻¹)
k_{-1}	Rate constant of desorption of organic pollutant from the bulk solution to the interfacial region of cavitation bubbles	(mg/L.min)
k_{app}	Apparent reaction rate constant in the different reaction order models	(mg/L.min or min ⁻¹ or L/mg.min for zero, first and second order)
k_D and $k'D$	Forward and backward rate constant of adsorption and desorption of dye	(min ⁻¹)
k_e	Rate constant of sonolytic catalyst	(min ⁻¹)
k_{hci}	Rate constants for oxidation dye by hole, $i = 1$ and 2	(min ⁻¹)
k_{hf} and k_{hb}	Forward and backward rate constants of recombination $\bullet\text{OH}$ to form H_2O_2	(min ⁻¹)
k_{OH} and k'_{OH}	Forward and backward rate constant of adsorption of $\bullet\text{OH}$	(min ⁻¹)
k_{oxi}	Rate constants for oxidation dye by $\bullet\text{OH}$ (presence of catalyst), $i = 1,2,3$ and 4	(min ⁻¹)
k_p	Rate constant of sonolysis water	(min ⁻¹)

k_{rc}	Rate constant of recombination hole and electron to generate heat	(min ⁻¹)
k_{rh1}	Rate constant of adsorbed •OH species oxidized by hole	(min ⁻¹)
k_{rh2}	Rate constant of adsorbed H ₂ O species oxidized by hole	(min ⁻¹)
k_{s1}, k_{s2} and k_{s3}	Rate constants for side reactions to form free radicals	(min ⁻¹)
λ	Wavelength of the light	(nm)
λ_x	Wavelength of the X-ray	(nm)
n	Number	Dimensionless
P	Pressure	(bar)
P_a	Pressure in the liquid (a sum of the hydrostatic and acoustic pressures)	(bar)
P_H	Hydrostatic pressure	(atm)
P_v	Pressure inside the bubble at its maximum size or the vapour pressure of the liquid	(bar)
P/P_0	Relative pressure	Dimensionless
ρ_L	Density of liquid	(kg/m ³)
r	Reaction rate of organic pollutant	(mg/L.min)
r_I	Rate of adsorption of the organic pollutant from the bulk solution to the interfacial region of cavitation bubbles	(mg/L.min)
r_{-I}	Rate of desorption of the organic pollutant from the interfacial region of cavitation bubbles to the bulk solution	(mg/L.min)
r_D	Reaction rate of dye	(mg/L.min)
R^2	Coefficient of determination	Dimensionless
R^2_{adj}	Adjusted coefficient of determination	Dimensionless
R_g	Universal gas constant	(J/mol.K)

R_m	Maximum radius of cavitation bubbles	(m)
R_{max} , R_{min} and R	Maximum reflectance, minimum reflectance and the reflectance at any intermediate photon energy	Dimensionless
S_c	Surface of catalyst	Dimensionless
T	Reaction temperature	(K)
T_{max}	Maximum temperature developed in the cavitation bubbles	(K)
T_0	Temperature of the bulk solution	(K)
T_p	Ultrasonic period	(s)
t	Irradiation time	(min)
t_t	Thickness of the semiconductor material	(m)
τ	Cavitation bubbles collapse time	(s)
W_A	Weight fraction of anatase	(%)
W_R	Weight fraction of rutile	(%)
x_i and x_j	Independent process variables, $i = 1,2$ and 3	Depands
y	Response of the degradation process	(%)
θ	Diffraction angle	Degree ($^{\circ}$)
θ_n	Ratio of the number of adsorbed organic pollutant molecules in the interfacial region to the maximum number of the adsorbable organic pollutant molecules	Dimensionless

SINTESIS DAN PENCIRIAN NANOTIUB TITANIUM DIOKSIDA BAGI PENGURAIAN SONO BERMANGKIN PENCELUP ORGANIK DALAM AIR SISA

ABSTRAK

Penguraian sono bermangkin bagi Rhodamin B telah dikaji menggunakan nanotuib titanium dioksida (NTs TiO₂) yang berbeza dengan pengolahan suhu dari 300 °C hingga 900 °C dengan tempoh masa 2 jam. Pencirian mangkin telah dikaji dengan menggunakan SEM, TEM, EDX, EA, AAS, XRD, spektroskopi Raman, FT-IR, penjerapan-penyahjerapan nitrogen, UV-vis DRS, TGA-DTA, pengukuran keupayaan Zeta dan XPS. Kesan terhadap aktiviti sono bermangkin dengan menggunakan nanopartikel TiO₂ atau pelbagai tersepuh NTs TiO₂ dan pelbagai parameter ujikaji termasuk pengunaan pelbagai pencelup organik (Congo Merah, Reaktif Biru 4, Metil Jingga, Metilena Biru dan Rhodamin B), kepekatan asal Rhodamin B 50–150 mg/L, dos mangkin 0.5–2.5 g/L, pH larutan 1–11, frekuensi ultrasonik 35 atau 130 kHz, kuasa ultrasonik 20–100 W, dos hidrogen peroksida (H₂O₂) 4–20 mM, suhu larutan 25–50 °C dan kewujudan udara terlarut telah diselidik untuk menentukan keadaan optimum. Keadaan optimum bagi penguraian sono bermangkin bagi Rhodamin B yang tertinggi (88.47 % selepas 2 jam) berlaku apabila 50 mg/L kepekatan asal Rhodamin B, 2 g/L dosej mangkin, pH larutan 7, frekuensi ultrasonik 35 kHz, kuasa ultrasonik 50 W dan 8 mM dosej H₂O₂ pada 45 °C ± 2 digunakan. NTs TiO₂ yang sedia ada diubahsuai dengan memperkenalkan urea kepada NTs TiO₂ pada nisbah molar N: Ti di antara 0.1–1.0. Pendopan urea pada N: Ti sama dengan 0.3 mangakibatkan kenaikan penguraian sono bermangkin bagi Rhodamin B kepada 86.75 % selepas 1 jam. Sementara itu, Fe-didopkan NTs TiO₂ pada nisbah molar Fe: Ti di antara 0.001–0.02 telah disediakan. Optimum Fe pendopan pada Fe: Ti sama dengan 0.005 menunjukkan keaktifan penguraian sono

bermangkin yang tertinggi (91.19 %) selepas 1 jam. Dipercayai bahawa pendopan logam dan bukan logam boleh menggalakkan luas permukaan tertentu yang besar, tenaga jalur luang yang rendah, permukaan kekosongan oksigen yang banyak dan aktif, bererti membaiki keaktifan sono bermangkin NTs TiO₂. Fe³⁺ yang dilarutkan boleh memangkin tindak balas serupa Fenton yang selanjutnya membaiki tindak balas penguraian sono bermangkin. Penguraian sono bermangkin bagi Rhodamin B mengikuti kinetik tertib pertama yang ketara dan tindak balas tersebut hampir mematuhi persamaan keserupaan model kinetik Langmuir-Hinshelwood. Kajian penggunaan mangkin semula menunjukkan bahawa pengurangan aktiviti mangkin, Fe-didopkan NTs TiO₂ adalah dalam 6.58 % selama empat kitaran berturut-turut dengan kehilangan Fe daripada permukaan mangkin yang minimum. Penguraian sono bermangkin bagi air sisa tekstil sebenar yang menggunakan Fe-didopkan NTs TiO₂ pada Fe: Ti sama dengan 0.005 telah diselidiki. Kecekapan penguraian yang terbaik boleh dicapai pada pH larutan 3, 6 g/L dosej mangkin, 40 mM dosej H₂O₂, frekuensi ultrasonik 35 kHz dan kuasa ultrasonik 50 W selepas 1 jam masa penjerapan diikuti dengan 3 jam masa penyinaran ultrasonik di bawah udara terlarut yang berterusan. Penyingkiran warna, COD and TOC masing-masing ialah 79.9 %, 59.4 % and 49.8 %.

**SYNTHESIS AND CHARACTERIZATION OF TITANIUM DIOXIDE
NANOTUBES FOR SONOCATALYTIC DEGRADATION OF ORGANIC
DYES IN WASTEWATER**

ABSTRACT

The sonocatalytic degradation of Rhodamine B was studied using titanium dioxide nanotubes (TiO_2 NTs) with various annealing temperatures ranging from 300 °C to 900 °C for 2 h. Characterizations of the catalysts were performed using SEM, TEM, EDX, EA, AAS, XRD, Raman spectroscopy, FT-IR, nitrogen adsorption-desorption, UV-vis DRS, TGA-DTA, zeta potential measurement and XPS. The effect of catalytic activity for TiO_2 nanoparticles (NPs) or various annealed TiO_2 NTs and various experimental parameters including the use of various organic dyes (Congo Red, Reactive Blue 4, Methyl Orange, Methylene Blue and Rhodamine B), initial concentration of Rhodamine B of 50–150 mg/L, catalyst dosage of 0.5–2.5 g/L, solution pH of 1–11, ultrasonic frequency of 35 or 130 kHz, ultrasonic power of 20–100 W, hydrogen peroxide (H_2O_2) dosage of 4–20 mM, solution temperature of 25–50 °C and the presence of dissolved air at 1 L/min were examined to determine the optimum conditions. The optimum conditions for sonocatalytic degradation of Rhodamine B (88.47 % after 2 h) occurred when the initial concentration of the dye was 50 mg/L, 2 g/L of TiO_2 NTs-300, solution pH of 7, ultrasonic power of 50 W, ultrasonic frequency of 35 kHz and H_2O_2 dosage was 8 mM at 45 °C ± 2. The as-prepared TiO_2 NTs was modified by introducing urea on TiO_2 NTs at molar ratios of N: Ti between 0.1–1.0. Urea doping at N: Ti equals to 0.3 led to an increment in the sonocatalytic degradation of Rhodamine B up to 86.75 % after 1 h. Meanwhile, Fe-doped TiO_2 NTs at molar ratios of Fe: Ti between 0.001–0.02 were prepared. Fe doping at Fe: Ti equals to 0.005 gave the highest sonocatalytic activity (91.19 %) after 1 h. It was believed that metal or non-metal doping could induce higher specific

surface areas, lower band gap energy, more active surface oxygen vacancies which significantly improved sonocatalytic activity. Leached Fe³⁺ could catalyze Fenton-like reaction to further improve the sonocatalytic reaction. The sonocatalytic degradation Rhodamine B followed apparent first-order kinetic reaction and the reaction was well fitted using an equation similar to Langmuir-Hinshelwood kinetic model. Catalyst reusability study revealed that the reduction in catalytic activity for Fe-doped TiO₂ NTs was within 6.58 % for the four successive cycles with minimum loss of Fe from the catalyst surface. The sonocatalytic degradation of real textile wastewater in the presence of Fe-doped TiO₂ NTs at Fe: Ti equals to 0.005 was also investigated. The best degradation was achieved at a solution pH of 3, 6 g/L of catalyst dosage, 40 mM of H₂O₂, an ultrasonic frequency of 35 kHz and an output power of 50 W after 1 h of adsorption followed by 3 h of ultrasonic irradiation under continuous dissolved air conditions. The color, COD and TOC removals were 79.9 %, 59.4 % and 49.8 %, respectively.

CHAPTER 1

INTRODUCTION

1.1. Water pollution in Malaysia

The problem of water pollution in Malaysia has been receiving increased attention. Figure 1.1 shows the decreasing number of clean rivers and an increase in the number of polluted rivers throughout 2006 to 2011. According to Malaysia Environment Quality Report (Department of Environment, 2011), the increasing number of cases of water pollution was due to the increasing sewage treatment plants and manufacturing industries. Among the industrial sources of water pollution, textile finishing wastewater accounts for 22 % of the total volume of industrial wastewater generated in Malaysia (Rakmi, 1993). Before 1993, biological processes were generally preferable for wastewater treatment due to the low cost and less usage of chemical reagents.

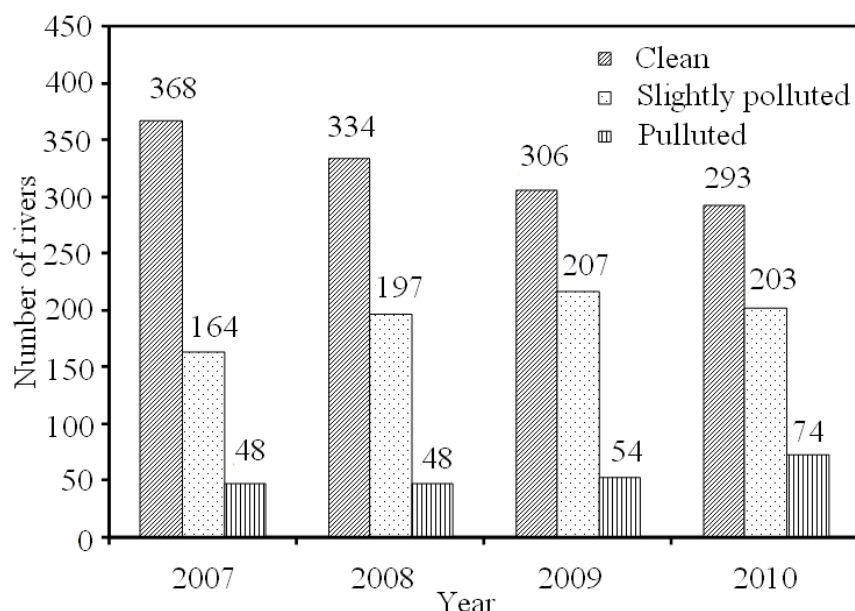


Figure 1.1: River water quality trend in Malaysia between 2007–2011 (Department of Environment, 2011).

1.2 Dye production, characteristics of textile industry effluent and its environmental impacts

Until recently, there is no data available on the exact amount of annual production of organic dyes in the world. However, more than 100,000 types of commercially available dyes exist and an annual worldwide production of synthetic dyes of nearly 1 million tons has been reported in the literature (Sinha *et al.*, 2013). An estimated 90 % of the total dyes production will end up in fabrics, while the remaining portion of the dyes will be used in leather, paper, plastic and chemical industries (Hameed *et al.*, 2007). It is estimated that 280,000 tons of textile dyes is discharged as industrial effluent every year worldwide (Ali, 2010).

The typical characteristics of wastewater from the effluents of the dyeing and finishing processes are shown in Table 1.1. It also shows the discharge quality standards which are stipulated in the Environmental Quality (Sewage Industrial Effluent) Regulations, 2009 to comply with the minimum requirements of the Environmental Quality Act 1974 (Department of Environment, 2011). Results in Table 1.1 show a range of values for each parameter involved which suggest a large variability of the wastewater quality from the dyeing and finishing processes.

The release of the persistent dyes structure with toxicity properties may cause negative impacts or hazards to human health and the ecosystem. The non-biodegradable nature of organic dyes and their high colour intensity are able to reduce aquatic diversity by blocking the passage of sunlight through the water (Jibril *et al.*, 2013). Moreover, some of them are capable of causing irritations to the skin, eyes, allergic dermatitis and respiratory tract (Merouani *et al.*, 2010b). The presence

of azo- and nitro-compounds in the structure of organic dyes has the possibility to generate aromatic amines if the textile effluent is incompletely treated. Aromatic amines are toxic, carcinogenic and mutagenic, so that some are capable of inducing cancer and tumor in human (Sun *et al.*, 2013).

Table 1.1: Typical characteristics of wastewater from a textile dyeing process and maximum effluent parameter limits for Standards A and B.

Parameters / component	Typical values	Standard A	Standard B	References
Temperature (°C)	30–80	40	40	(Lau and Ismail, 2009)
pH	2–10	6.0–9.0	5.5–9.0	(Verma <i>et al.</i> , 2012)
Biochemical oxygen demand (BOD_5) (mg/L)	110–5,600	20	50	(Verma <i>et al.</i> , 2012)
Chemical oxygen demand (COD) (mg/L)	2–5 x BOD_5	50	100	(Kaushik and Malik, 2009)
Total suspended solids (mg/L)	50–23,9	50	100	(Verma <i>et al.</i> , 2012)
Chromium hexalent (mg/L)	0.35–	0.05	0.05	(Kaushik and Malik, 2009)
trivalent (mg/L)	170	0.20	1.0	(Kaushik and Malik, 2009)
Copper (mg/L)	0.12–4.20	0.20	1.0	(Kaushik and Malik, 2009)
Nickel (mg/L)	0.10–0.96	0.20	1.0	(Kaushik and Malik, 2009)
Zinc (mg/L)	0.10–58	1.0	1.0	(Kaushik and Malik, 2009)
Phosphorous (mg/L)	0.3–15	n.d.	n.d.	(Lau and Ismail, 2009)
Nitrite (NO_2^-) (mg/L)	0.2–28	0.4	1.0	(Vilar <i>et al.</i> , 2011)
Nitrate (NO_3^-) (mg/L)	7–74	7.0	10.0	(Saeed and Sun, 2013)
Colour (Pt/Co)	> 300	*	*	(Lau and Ismail, 2009)

*The liquid effluent should not be coloured.

Standard A for discharge upstream of drinking water take-off.

Standard B for inland waters.

Five types of dye are investigated in this research work as shown in Table 1.2.

The Ecological and Toxicological Association of the Dyestuffs Manufacturing Industry in year 1974 found that basic dyes and diazo direct dyes have the highest

toxicity among 4000 dyes tested (Robinson *et al.*, 2001). It is reported that basic dyes have high brilliance and colour intensity even in a very low concentration (Merouani *et al.*, 2010b). **One of** the main organic dyes used as a model pollutant in many studies is Rhodamine B. Meanwhile, acid and reactive dyes with azo or anthraquinone group are toxic to some organisms and may cause direct destruction on many creatures in water (Ahmad and Hameed, 2010).

Table 1.2: Chemical structures and classifications of organic dyes used in this study (Tangestaninejad *et al.*, 2008; Jamalluddin and Abdullah, 2011).

Dyes	Classification	Chemical structure
Congo Red	Anionic direct diazo	
Reactive Blue 4	Anionic reactive anthraquinone	
Methyl Orange	Anionic acid monoazo	
Rhodamine B	Cationic basic xanthene	
Methylene Blue	Cationic basic thiazine	

1.3 Colour removal techniques

The presence of dyes in wastewater effluent is highly undesirable. As such, several treatment methods which include physical, chemical and biological treatments have been applied before discharge to the environment. Some of the dye conventional removal techniques with their respective limitations in textile industry have been discussed. Adsorption using commercially available activated carbon is very expensive and the need of regeneration becomes its limitation to be widely used. Thus, many efforts have been made to search for lower cost waste material adsorbents such as bamboo waste (Ahmad and Hameed, 2010), rejected tea (Nasuha and Hameed, 2011), coffee residues (Kyzas *et al.*, 2012), waste newspaper (Zhang *et al.*, 2013), oil palm empty fruit bunch (Sajab *et al.*, 2013) and pineapple peel (Foo and Hameed, 2012). Adsorption may be effective for decolourization but the process only involves a phase transfer of pollutants to other secondary wastes that subsequently require additional treatment or proper disposal procedure.

Filtration technology to treat textile effluents includes microfiltration (Baburaj *et al.*, 2012), ultrafiltration (Aouni *et al.*, 2012), nanofiltration (Ellouze *et al.*, 2012; Shao *et al.*, 2013; Zheng *et al.*, 2013) and reverse osmosis (Liu *et al.*, 2011; Kurt *et al.*, 2012). However, the disadvantages of this method are such as it can only be applied on small wastewater flow rate, high cost of membrane formation, high working pressure to push the wastewater flow through membrane filtration and inability to reduce dissolved solid content. Thus, this method requires frequent cleaning and replacement of the modules to maintain effectiveness in removing of organic dyes.

Biodegradation of organic dyes is very difficult as the structure of organic dyes is usually very complex, stable and sometimes it contains long-lasting colourants. Nevertheless, the possible microorganisms used for biodegradation dyes are fungi (Lade *et al.*, 2012), bacteria (Cui *et al.*, 2012), yeasts (Qu *et al.*, 2012) and algae (Daneshvar *et al.*, 2012; Baldev *et al.*, 2013). The problems which limit their application in industry are the toxicity of dyes toward the organisms used in the aerobic biological process and long hydraulic retention time so that larger tank is generally required. On the other hand, the main problem which occurs in colour removal under anaerobic condition is the production of aromatic amine during azoreductase cleavage of the azo bond which is more toxic than the dye itself (Qu *et al.*, 2012).

Chemical treatment includes coagulation and flocculation using aluminium sulfate, lime and ferric salts (Verma *et al.*, 2012). However, the handling of large volume of concentrated sludge produced would increase the capital cost for wastewater treatment. Other limitations that need to be considered for this technique are the high cost of coagulating or flocculating agent and the pH dependency for effective dye removal. Meanwhile, ion exchange method is ineffective to remove several types of dye simultaneously. Both cationic (basic dyes) and anionic (acid, direct, reactive dyes) types can only be removed effectively using different resins (Makhoukhi *et al.*, 2010; Wawrzkiewicz, 2012; Wawrzkiewicz, 2013). Other disadvantages are such as low removal in the case of nonionic dyes (disperse dyes), diffusion limitation that can affect reaction rate while the use of organic solvent for regeneration is very expensive (Robinson *et al.*, 2001).

Chemical oxidation for complete mineralization is a focus area in advanced oxidation processes (AOPs). Fenton and Fenton-like treatments have been reported for the ability to decolourize a wide range of textile dyes in rather short reaction times (Zhu *et al.*, 2012). The major disadvantage of this method is sludge generation through the flocculation of the reagent and the dye molecules. Ozonation of textile effluents results in efficient colour removal, enhanced biodegradability and reduction in non-biodegradable COD (Oller *et al.*, 2011). Ozonation can rapidly decolourize water-soluble dyes but takes a longer time to oxidize non-soluble dyes (van der Zee, 2002). It also has a relatively short life time of approximately 20 min (Buntat *et al.*, 2009).

On the other hand, photocatalytic and sonocatalytic processes are able to mineralize dye molecules to carbon dioxide (CO_2) and water (H_2O). Both types of degradation rate can be enhanced by adding hydrogen peroxide (H_2O_2) to increase the formation of hydroxyl radical ($\cdot\text{OH}$). $\cdot\text{OH}$ has become an important oxidant due to its high reactivity and lack of selectivity towards organic compounds. The disadvantage of the photocatalytic process is the low penetration ability (several millimeters) in water medium. However, higher penetrating ability (25–30 cm) in water medium can be achieved through the use of ultrasonic irradiation (Zhang and Oh, 2010). Hence, there has been an increase of interest in the use of ultrasound to destroy organic contaminants that present in wastewater.

1.4 Problem statement

The main issue faced by textile industry is the incomplete degree of fixation of dyes that leads to water pollution during textile fiber processing. Most of these

organic dyes can cause irritation to the skin, eyes and systemic effects including blood changes, gastrointestinal tract and respiratory tract. Besides, the presence of benzene ring in the dye structure always causes conventional treatment process to be ineffective in destroying the organic pollutants (Wang *et al.*, 2007a). Therefore, the most promising way is the application of AOPs to oxidize those hazardous organic pollutants. Among AOPs, photocatalytic degradation is a plausible method but it has limited practical application in treating heavily coloured effluents due to low penetration of the ultraviolet (UV) light. Hence, the application of ultrasonic irradiation could overcome the main drawbacks of UV light.

However, the successful application of titanium dioxide (TiO_2) is still constrained by the wide band gap energies (3.2 or 3.0 eV in the anatase or rutile phase, respectively) (Wang *et al.*, 2008b). Most of the research works done so far do not address the optimum conditions for sonocatalytic degradation of dye. Optimization of sonocatalytic degradation of dyes using response surface methodology is rarely reported. In addition, reaction kinetic for sonocatalytic degradation of dye is yet to be well established. The activity of TiO_2 is known to decrease dramatically for the reapplication in the sonocatalytic or photocatalytic degradation. Lastly, information on the sonocatalytic treatment for real textile wastewater is quite scarce as most of the research works done are merely limited to the removal of specific dyes from pure dye solutions.

Therefore, TiO_2 nanotubes (NTs) catalyst is prepared by hydrothermal treatment before treating the organic dye in aqueous solution under ultrasonic irradiation. Besides, TiO_2 NTs have improved properties as compared to TiO_2 NPs

such as high aspect ratio that can result in higher surface area. Then, different effects of operating parameters on the sonocatalytic degradation of dye in the presence of TiO₂ NTs are worth investigation and elucidation. Optimum conditions and interaction effects between parameters to achieve higher efficiency of sonocatalytic degradation of the dye should be identified. The purposes of introducing iron or nitrogen ions into TiO₂ NTs are to narrow the band gap energy of TiO₂ NTs and to increase the transport of separated electron throughout the nanotubes. The catalytic activity and stability of catalyst developed during ultrasonic irradiation should also be evaluated. A reliable reaction kinetic for degradation of dye needs to be proposed. Lastly, the feasibility of oxidative decolourization of textile wastewater through adsorption followed by ultrasonic irradiation in the presence of Fe-doped TiO₂ NTs should be evaluated.

1.5 Research objectives

The main goal of this study is to develop a novel TiO₂ catalyst as a sonocatalyst for repeated usage in sonocatalytic degradation of dyes without suffering from significant activity decrease. Specific objectives of this study include the following:

- i. To synthesize and characterize TiO₂ NTs using hydrothermal synthesis and annealing with different temperatures in order to accelerate the sonocatalytic degradation reaction of Rhodamine B in water.
- ii. To demonstrate the process behaviour of the sonocatalytic degradation process under various operating conditions with the objective of identifying the most suitable and optimum reaction conditions.

- iii. To study the characteristics of doped TiO₂ NTs by incorporating nitrogen at molar ratios of N: Ti between 0.1–1.0 or iron ions at molar ratios of Fe: Ti between 0.001–0.02 in order to enhance the sonocatalytic activity.
- iv. To study the reusability of the un-doped and Fe-doped TiO₂ NTs covering the evaluation of the sonocatalytic activity during repeated use and its stability after ultrasonic irradiation through various suitable characterization methods.
- v. To study the reaction kinetic orders, Langmuir-Hinshelwood kinetic to model the sonocatalytic degradation process and performance of sonocatalytic degradation using real textile industry wastewater.

1.6 Research scope

TiO₂ NTs was synthesized through a hydrothermal method in a concentrated alkali solution. Effects of various heat treatments (300 °C, 500 °C, 700 °C and 900 °C) on the characteristics of the TiO₂ NTs sonocatalysts and their consequent effects on the catalytic activity were investigated. TiO₂ NPs and TiO₂ NTs were characterized using scanning electron microscopy (SEM), transmission electron microscopy (TEM), energy dispersive X-ray (EDX) analysis, X-ray diffraction (XRD), Raman spectroscopy, Fourier transformed infrared (FT-IR) spectroscopy, nitrogen adsorption-desorption isotherm, UV-vis diffuse reflectance spectroscopy (UV-vis DRS), thermal gravimetric analysis-differential thermal analysis (TGA-DTA) and zeta potential measurements.

Then, a series of experiments were conducted using TiO₂ NPs and different types of heat-treated TiO₂ NTs catalysts to compare the degradation performance of Rhodamine B. This is followed by sonolytic and sonocatalytic degradation of various

organic dyes including Congo Red, Reactive Blue 4, Methyl Orange, Methylene Blue and Rhodamine B. The process variables investigated include the effect of initial concentration of Rhodamine B (50–150 mg/L), the effect of catalyst dosage (0.5–2.5 g/L), the effect of solution pH (pH 1–pH 11), the effect of ultrasonic frequency (35 kHz or 130 kHz), the effect of ultrasonic power (20–100 W), the effect of solution temperature (25 °C–50 °C), the effect of H₂O₂ dosage (4–20 mM) and finally the effect of the presence of dissolved air at 1 L/min. Each of the range of variables chosen was based on reports in the literature and through the process of trial and error during preliminary study. Besides, the optimum conditions of three process variables for the sonocatalytic degradation of Rhodamine B were obtained from DoE approach. The selected three most significant variables were the initial concentration of Rhodamine B (30–70 mg/L), catalyst dosage (1.5–2.5 g/L) and ultrasonic power (40–80 W). Then, the concentrations of liquid sample were collected and measured using UV-vis spectrophotometer.

A range of C-N codoped TiO₂ NTs (molar ratios of N: Ti were 0.1, 0.3, 0.5 and 1.0) were synthesized using hydrothermal and calcination methods. These catalysts were characterized through SEM, TEM, EDX, elemental analysis (EA), XRD, FT-IR, nitrogen adsorption-desorption measurement, UV-vis DRS, TGA-DTA and X-ray photoelectron spectroscopy (XPS). The sonocatalytic activities of C-N codoped TiO₂ NTs were investigated under optimum conditions. This is followed by the characteristics and catalytic activities study of Fe-doped TiO₂ NTs with molar ratios of Fe to Ti were 0.001, 0.005, 0.01 and 0.02. The possible mechanism for sonocatalytic activation of Fe-doped TiO₂ NTs was proposed. Meanwhile, the

generated intermediate products were detected through FT-IR analysis and gas chromatograph coupled with mass spectrometry (GC/MS).

On the other hand, characterization tests and evaluation of sonocatalytic activities on the reused TiO₂ NTs and Fe-doped TiO₂ NTs catalysts were also conducted. The characterization methods comprised of SEM, TEM, EDX, XRD, nitrogen adsorption-desorption isotherm, atomic absorption flame emission spectroscopy (AAS) and TGA for four catalytic cycles. The kinetic reaction and kinetic model for sonocatalytic degradation reaction of Rhodamine B was included. Then, the performance of sonocatalytic degradation of real textile wastewater was performed. All this information will be useful in promoting a better understanding of the optimum conditions for sonocatalytic degradation of organic dyes.

1.7 Organization of thesis

This thesis consists of five chapters. Chapter 1 gives brief introduction to water pollution especially in Malaysia, dye production, characteristics of textile industry effluent and its environmental impacts. Various types of wastewater treatment method with their advantages and disadvantages are discussed. Problem statements are then given after reviewing the scenario of current wastewater treatment methods. This section also highlights current problems faced by the textile industry and the importance of this research project. The objectives of this research project are then carefully divided with the aim of solving the problems faced by the textile industry. Finally, the organization of this thesis section highlights the contents of each chapter.

Chapter 2 gives an overall review of various research works reported in the literature in this research area. A review on the fundamentals of ultrasound, ultrasonic reaction system as well as sonolytic kinetic mechanism of water molecules is presented. The recent works on the sonocatalytic degradation of organic dyes by using TiO₂ are given. Next, a review on the synthesis methods for TiO₂ NTs, formation mechanism, post calcination and modifications of TiO₂ NTs is also presented. This is followed by the review of characterization techniques used to study the properties of the un-doped and doped TiO₂ NTs. Besides, the effects of various operating variables on the performance of the sonocatalytic degradation of organic dyes and the optimization study by means of DoE approach are reviewed. The mechanism of oxidation degradation of Rhodamine B is thoroughly reviewed and subsequently, followed by the catalyst reusability studies. The reaction kinetic and Langmuir-type model based on heterogeneous reaction systems for sonocatalytic degradation of organic dye are reviewed.

In Chapter 3, chemicals, materials and methodologies involved in this study are described in detail. It starts by listing all the chemicals and reagents used with their purity, followed by the overall flow of the research work and experimental setup. The preparation and characterizations of TiO₂ NPs and TiO₂ NTs, optimization studies using conventional one factor at a time and DoE approach are included. The following section describes the preparation, characterizations and sonocatalytic activities of C-N codoped and Fe-doped TiO₂ NTs. The details on the collection of liquid sample for determination of concentration and intermediate product analysis are given. Then, the catalyst reusability studies, reaction kinetic and

Langmuir-type model study are presented. This is followed by describing the performance of sonocatalytic degradation of real textile wastewater.

Chapter 4 is the most important chapter in the thesis. It encompasses the detail discussion on the results obtained in the present research work. The first section presents the characterizations of prepared TiO₂ NPs and annealed-TiO₂ NTs catalysts. This is followed by a study on the effect of parameters such as initial concentration of Rhodamine B, catalyst dosage, solution pH, ultrasonic frequency, ultrasonic power, H₂O₂ dosage, solution temperature and the use of dissolved air. DoE approach is used to optimize three significant variables that are, initial concentration of Rhodamine B, catalyst dosage and ultrasonic power. The next section reports on the preparation, characterizations and sonocatalytic activities of C-N codoped and Fe-doped TiO₂ NTs. The formation of intermediate products after sonocatalytic degradation of Rhodamine B is also studied. The reusability of catalyst is evaluated based on changes in the characteristics and catalytic activity in sonocatalytic degradation of Rhodamine B. Besides, reaction kinetics based on Langmuir-type model fitting for the sonocatalytic degradation is also presented. In the final section, adsorption followed by sonocatalytic degradation of real textile wastewater using Fe-doped TiO₂ NTs is investigated.

Chapter 5 gives a summary on the important findings made in this research work. Suggestions and recommendations to improve the present work as well as the future extension to the current study are also presented.

CHAPTER 2

LITERATURE REVIEW

2.1. Fundamentals of ultrasound

Ultrasound is defined as a sound wave with a frequency that is greater than the upper limit of human hearing ability, approximately 20 kHz and wavelength is about 75 mm (Khanal *et al.*, 2007; Thangavadivel *et al.*, 2009). The transmission of ultrasound waves that impose a sinusoidally varying pressure across an aqueous phase can cause the occurrence of cavitation as shown in Figure 2.1 (Leong *et al.*, 2011). Cavities (tiny micro bubbles) can be created during the expansion cycle with sufficient intensity with the distance between water molecules exceeding the critical molecular distance (10^{-8} m) (Vajnhandl and Majcen Le Marechal, 2005). During the expansion cycle, bubbles may grow rapidly and cause the dissolution of gases in the liquid to diffuse into the bubbles. Gasses that have diffused into the bubbles will be expelled into the fluid during the compression cycle.

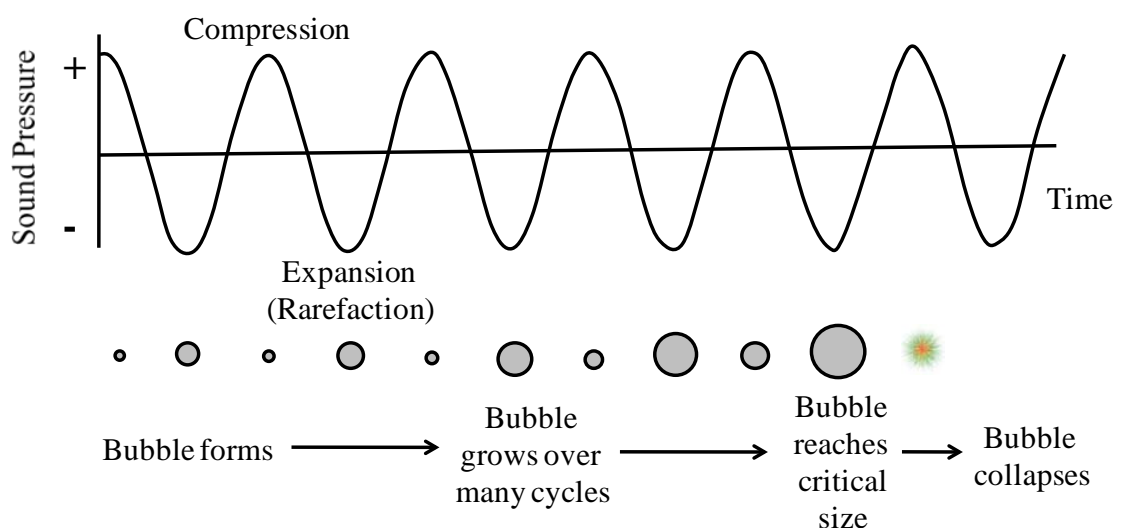


Figure 2.1: Graphical summary of the event of bubble formation, bubble growth and subsequent collapse over several acoustic cycles (Leong *et al.*, 2011).

Cavitation bubbles will grow over a few cycles by entrapping most of the vapour from the medium to reach a critical size before the implosion of the bubbles occurs as shown in Figure 2.2 (Suslick, 1989). The radius of the bubble before collapse when irradiated at 20 kHz is estimated to be in the order of several hundred micrometers. The time scale for the collapse of bubbles is less than 100 nanoseconds (Kotronarou *et al.*, 1992). The effective lifetime is less than 2 microseconds after which they start to collapse (Suslick, 1990). In summary, the phenomenon of cavitation consists of the repetitive and distinct three steps: formation (nucleation) and rapid growth (expansion) during the compression/ rarefaction cycles until they finally reach a critical size. After that, they start to undergo violent collapse (implosion) in the liquid (Ghodbane and Hamdaoui, 2009).

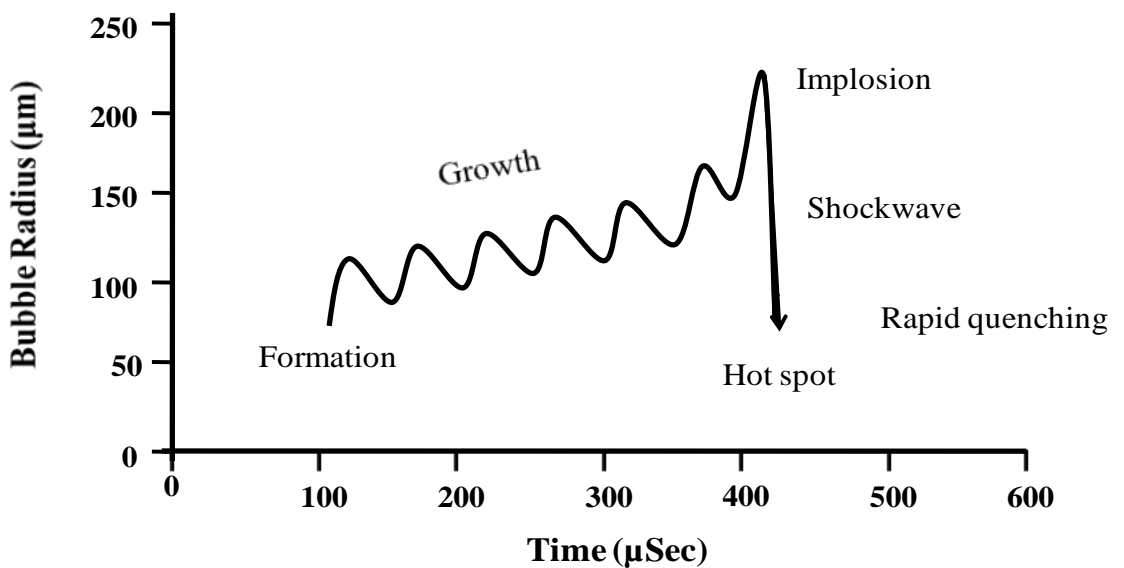


Figure 2.2: Formation, growth and implosion of cavitation bubble in aqueous solution with ultrasonic irradiation bubbles (Suslick, 1989).

2.1.1. Sonolytic kinetic mechanism of water molecules

The presence of dissolved oxygen (O_2) is reported to improve sonolysis reactions. However, it is not necessary for water (H_2O) sonolysis because sonolysis can proceed in the presence of any gas such as air, nitrogen, argon and hydrogen (Adewuyi, 2001). Ultrasound will induce the splitting of water molecules with the presence of dissolved oxygen and causes reactions (2.1)–(2.12) to occur (Adewuyi, 2001; Zhou *et al.*, 2013). In these reactions, '))' denotes the ultrasonic irradiation.

Thermal dissociation of H_2O and dissolved O_2 molecules in the cavities will convert them into reactive species such as $\cdot OH$, hydrogen ($\cdot H$), $\cdot O$ and hydroperoxyl radicals ($\cdot OOH$) (reactions (1)–(5)). After that, the reactive radicals can enter into a variety of chemical reactions in the cavitation bubble and/or in the bulk solution. In the absence of any solutes, these primary radicals could recombine to form H_2O , $\cdot O$ and O_2 and then released into the bulk solution (reactions (2.6)–(2.8)).

H_2O_2 will be formed outside the hot bubbles or at the cooler interface as a consequence of $\cdot OH$ and $\cdot OOH$ recombination (reactions (2.9) and (2.10)). On the other hand, the $\cdot H$ and $\cdot OH$ species may further react with H_2O_2 as shown in reactions (2.11)–(2.12). The radicals ($\cdot OH$ and $\cdot OOH$) may also reach the liquid–bubble interface and may pass into bulk solution where they can react with solutes.





2.1.2. Ultrasonic reaction systems

There are three possible reaction zones in sonolysis liquid (Ghodbane and Hamdaoui, 2009; Moumeni and Hamdaoui, 2012) i.e. inside of the cavitation bubble, interfacial region between cavitation bubbles and bulk liquid and in the bulk solution. The temperatures of the interior and interfacial regions of the cavitation bubbles in alkanes as determined by Suslick *et al.* (1986) were 5200 K and 1900 K, respectively. Meanwhile, the temperature of the interfacial region of cavitation bubbles in the water supercritical phase was only 647 K (Hua *et al.*, 1995).

The reaction pathway depends on the volatility and hydrophobicity of the compound (Moumeni and Hamdaoui, 2012). Hydrophobic compounds with high volatility can be thermally decomposed inside the cavitation bubbles while hydrophilic with less or non-volatile organic compounds can be indirectly decomposed in the bulk liquid phase through the reaction with reactive radicals such as $\cdot\text{OH}$ (Son *et al.*, 2012). The highly reactive radicals could diffuse from the

cavitation bubbles to the interfacial region and bulk solution when large temperature gradient exists (David, 2009).

On the other hand, nano-particles with sizes less than those of cavitation bubbles have higher cavitation erosion resistant and are easier to approach the interfacial region (bubbles surface) during the expansion cycles of ultrasound (Lampke *et al.*, 2008; Morel *et al.*, 2008). Figure 2.3 (a) shows the effective reaction zone (interfacial region) where very high concentration of $\bullet\text{OH}$ is achieved after the bubbles collapse (Morel *et al.*, 2008). The concentration that could be reached is estimated to be as high as 4 mM (Lu and Weavers, 2002).

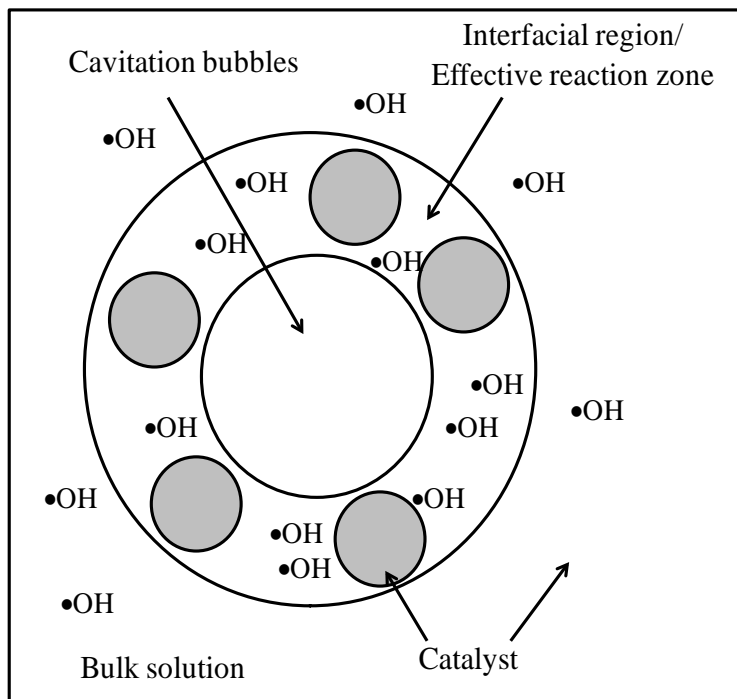


Figure 2.3: Schematic representations of effective reaction zone in cavitation bubbles (Morel *et al.*, 2008).

The asymmetric collapse of cavitation bubbles near the micro-particle surface will generate high-speed micro-jets of liquid in the order of 100 m/s (Suslick, 1990).

This may cause direct erosion (damage) on the particle's surface and de-aggregation of particles (Eren, 2012). Besides, the solid particles will experience a decrease in particle size and an increase in reactive surface area available for the subsequent reaction. The severity of the cavitation erosion that cause pitting and cracking of the particle surface is strongly influenced by the solid particle size (Chen *et al.*, 2007b).

2.2. Heterogeneous sonocatalytic degradation using titanium dioxide (TiO_2)

Many efforts have been devoted to improve the degradation efficiency in sonolysis processes. It is generally known that this process can be accelerated by the addition of various kinds of catalyst such as zinc oxide (ZnO) (Wang *et al.*, 2008a), iron oxide (Fe_2O_3) (Chen *et al.*, 2010) and copper oxide (CuO) (Zhang *et al.*, 2012). The presence of heterogeneous catalyst represents weak points in the liquid for nucleation of the cavitation bubbles to occur (Eren, 2012). The catalyst can enhance the dissociation of H_2O molecules (reaction 1) to increase the number of free radicals generated, thereby increasing the rate of degradation of the organic compound.

The most common type of catalyst to be used as sonocatalyst is TiO_2 due to its advantages such as inexpensive, non-toxic, chemically stable and long durability (Nakata and Fujishima, 2012). Table 2.1 summarizes reported findings on ultrasonic conditions, important conclusions and performance of TiO_2 -based catalysts for enhancement of the degradation of recalcitrant organic compounds. It is generally reported that the optimum amount of catalyst is influenced by many factors such as initial dye concentration, irradiation intensity and type of catalyst (Gaya and Abdullah, 2008). Besides, it can be seen that there are optimum dopant/composite concentration of metals to achieve the highest degradation rate of organic pollutants.

Table 2.1: Sonocatalytic degradation of recalcitrant organic compounds by TiO₂-based catalysts.

No	Organic pollutants	Catalyst	Optimum reaction conditions	Important findings	References
1	Methyl Orange (MO)	(i) Rutile TiO ₂ (ii) Transition crystal TiO ₂	100 ml of 10 mg/l MO; 0.1 g of TiO ₂ ; 40 kHz; 50 W ^a ; 80 min	(i) The degradation rate of transition crystal TiO ₂ (75 %) was higher than that of rutile TiO ₂ (55.9 %); (ii) Inorganic anions: NO ₂ ⁻ , NO ₃ ⁻ , SO ₄ ²⁻	(Wang <i>et al.</i> , 2007b)
2	Basic Blue 41 (BB 41)	Nano-sized TiO ₂	100 ml of 15 mg/l BB 41; 0.01 g of TiO ₂ ; 35 kHz; 160 W ^a ; 3 h	(i) H ₂ O ₂ accelerated the degradation rate from 18 to 62 %; (ii) Apparent first-order reaction kinetics; (iii) Products: urea, nitrate, formic acid, acetic acid and oxalic acid	(Abbasi and Asl, 2008)
3	Phenol	Mixture of anatase and rutile TiO ₂	7 l of 10 g/l phenol; 2 g/l of TiO ₂ ; 25 kHz; 1 kW ^a ; 206.3 kJ ^b ; 3 h	(i) The degradation rate was increased from 12.2 to 37.8 % in the presence of UV irradiation, TiO ₂ and H ₂ O ₂ . (ii) No intermediate products were reported.	(Khokhawala and Gogate, 2010)
4	2-chloro-5-methyl phenol (CMP)	Degussa P25 TiO ₂	100 ml of CMP; 0.6-0.9 g of coal ash; 33 kHz; 1225 W ^b ; 2 h	(i) The degradation rate was increased from 35 to 75 % in the presence of TiO ₂ and H ₂ O ₂ ; (ii) Apparent first-order reaction kinetics; (iii) The degradation rate was increased from 12 to 33 % in the presence of 100 mg/l of carbon tetrachloride (CCl ₄) and decreased in the presence of 1 % of methanol.	(Nalini Vijaya Laxmi <i>et al.</i> , 2010)
5	Methyl parathion (MP)	Mixture of anatase and rutile TiO ₂	100 ml of 20 ppm MP; 400 ppm of TiO ₂ ; 20 kHz, 230 – 270 W ^a ; 1 h	(i) The degradation rate was increased from 10.2 to 73.3 % in the presence of TiO ₂ , CCl ₄ , H ₂ O ₂ and fenton reagent; (ii) Apparent first-order reaction kinetics	(Shriwas and Gogate, 2011)
6	Dinitrotoluene/ Trinitrotoluene	Nanometer rutile TiO ₂	300 ml of 200 mg/l wastewater; 2 g/l of TiO ₂ ; 20 kHz; 70 – 210 W ^a ; 6 h	(i) The degradation rate was enhanced from 28 to 89 % in the presence of TiO ₂ and oxygen dosage; (ii) Apparent first-order reaction kinetics; (iii) Products detected: toluene, mononitrotoluene, trinitrobenzene	(Chen and Huang, 2011)

Table 2.1 (Continued)

No	Organic pollutants	Catalyst	Optimum reaction conditions	Important findings	References
7	Methylene Blue (MB)	C-Cr codoped-TiO ₂	100 ml of 10 mg/l MB; 0.1 g of catalyst; 40 kHz; 80 W ^a ; 3 h	(i) Sonocatalytic degradation efficiency of C-Cr-TiO ₂ (C: 1 wt. %, Cr: 1wt. %) was the highest (80 %), followed by undoped-TiO ₂ (43 %), C-TiO ₂ (20 %) and Cr-TiO ₂ (22 %); (ii) No products and reaction kinetic were reported	(Zhang, 2012)
8	Azo Fuchsine (AF)	(i) Cr ³⁺ -TiO ₂ (ii) Co ³⁺ -TiO ₂	50 ml of 10 mg/l AF; 0.05 g of catalyst; 40 kHz; 50 W ^a ; 2 h	(i) The degradation rate of 0.25 mol % Cr ³⁺ -TiO ₂ was 89 % followed by Co ³⁺ -TiO ₂ (45 %) and undoped TiO ₂ (26 %); (ii) Apparent first-order reaction kinetics; (iii) Inorganic anions: NO ₂ ⁻ , NO ₃ ⁻ , SO ₄ ²⁻	(Wang <i>et al.</i> , 2009b)
9	Reactive Black 5 (RB5)	(i) TiO ₂ (ii) CdS (iii) CdS/TiO ₂	50 ml of 100 mg/l RB5; 0.05 g of catalyst; 20 kHz, 41 W ^b ; 1 h	(i) The degradation rate of TiO ₂ /CdS (6:1) was the highest (94 %), followed by CdS (64 %) and TiO ₂ (80 %); (ii) Inorganic anions: NO ₃ ⁻ , SO ₄ ²⁻	(Ghows and Entezari, 2011)
10	Acid Red B (ARB)	(i) CeO ₂ /TiO ₂ (ii) SnO ₂ /TiO ₂ (iii) ZrO ₂ /TiO ₂	50 ml of 10 mg/l ARB; 0.01 g of catalyst; 40 kHz; 50 W ^a ; 100 min	(i) The degradation rate of CeO ₂ /TiO ₂ (4:1) was 87 %, followed by SnO ₂ /TiO ₂ (65 %) and ZrO ₂ /TiO ₂ (40 %); (ii) Apparent first-order reaction kinetics	(Wang <i>et al.</i> , 2010b)
11	MO	InVO ₄ /TiO ₂	50 ml of 1x10 ⁻⁵ M solution; 0.03 g of catalyst; 28 kHz; 60 W ^a ; 1 h	(i) InVO ₄ /TiO ₂ at 1:50 and 1:25 have highest sono- (80 %) and photo-catalytic activities (45 %), respectively; (ii) The degradation rate was increased in the presence of different oxidation reagents	(Min <i>et al.</i> , 2012)
12	ARB/ Methyl Violent/ Violent/ Rhodamine B	(i) TiO ₂ (ii) Al ₂ O ₃ / TiO ₂ (iii) Y ₂ O ₃ / TiO ₂ (iv)Fe ₂ O ₃ / TiO ₂	100 ml of 10 mg/l dyes solution; 40 kHz; 50W ^a ; 100 min	(i) The degradation rate of Al ₂ O ₃ / TiO ₂ (4:1) was the 79 %, followed by Y ₂ O ₃ /TiO ₂ (62 %), Fe ₂ O ₃ /TiO ₂ (50 %) and TiO ₂ (46 %); (ii) The degradation rate of ARB was 79 %, followed by Methyl Violent (60 %) and Rhodamine B (27 %)	(Chen <i>et al.</i> , 2011)

Note: ^aabsolute power (where no data on specific acoustic power is given); ^bacoustic power determined by calorimeter method

Although the modification with transition metals is yet to be practical industrially, it provides a future for a successful and effective alternative in sonocatalytic degradation.

There has been no ready-made mechanism and satisfying explanation yet on the sonocatalytic degradation process in the presence of catalyst under ultrasonic irradiation. However, it is often reported that the possible mechanism should be based on both light and heat energies that come from the ultrasonic cavitation effect. The implosion of micro-bubbles will result in a short local sonoluminescence and hot spot conditions (localized generation of extreme conditions, high temperature and high pressure) (Guo *et al.*, 2011; Wang *et al.*, 2011c). The sonoluminescence can result in the formation of the light flash of average photon energy of 6 eV (Vinu and Madras, 2009). These light and energy are sufficient to excite the catalyst i.e. TiO₂ acting as a sonocatalyst, which causes some electrons to be transferred from the valence band to the conduction band. At the same time, the hole-electron pairs are formed. These holes and electrons will react with the absorbed H₂O molecules on the surface of TiO₂ particles and molecular O₂ dissolved in aqueous solution, respectively, to produce •OH and superoxides radical anion (•O₂⁻). These highly reactive species are capable to attack various organic pollutants in wastewater.

2.3. TiO₂ nanotubes (NTs) catalyst

In terms of practical use, further development to improve the sonocatalytic activity of TiO₂ NPs is of great interest to current researchers. Three-dimensional (3D) TiO₂ NPs exhibits scattering effect of free electrons and electron trapping at the interface because of the formation of grain boundaries (Wang and Lin, 2010). It is

well-known that grain boundaries often act as hole-electron recombination sites, thereby reducing electron mobility and exhibiting slow electron transport (Wang *et al.*, 2009c; Wang and Lin, 2010).

One-dimensional (1D) nanotubes have attracted extraordinary attention due to the unique physical and chemical properties. TiO₂ NTs are expected to facilitate electron transport due to the interconnections between nanotubes are greatly decreased in comparison with accumulated nanosized particles (Adachi *et al.*, 2004; Tan and Wu, 2006). Fast electron transport throughout the 1D channel may account for the excellent charge separation (Feng *et al.*, 2008). Mor *et al.* (2006) reported that the TiO₂ NTs array exhibited superior electron lifetimes than TiO₂ NPs. In addition to the effect on electron transport, TiO₂ NTs enhance the light scattering and harvesting due to the high length to diameter ratio (Wang *et al.*, 2009c). Besides, the special feature of TiO₂ NTs with its large surface area provided by inner and outer surfaces of the tubular structure is able to adsorb and reacts with more organic pollutant molecules. Thus, the use of highly crystalline anatase nanotubes is anticipated to be one of the most promising ways. To our knowledge, sonocatalytic degradation using TiO₂ NTs has yet to be reported.

Currently, the most common techniques to synthesize TiO₂ NTs comprised of template-assisted method, electrochemical anodization and hydrothermal method. Hoyer (1996) was the first researcher report to the preparation of TiO₂ NTs via a template-assisted method. Thereafter, the production of TiO₂ NTs materials was also reported by Kasuga *et al.* (1998) via hydrothermal method. Meanwhile, Gong *et al.* (2001) reported that uniform TiO₂ NTs arrays was obtained through anodic oxidation